RSC Applied Interfaces

ROYAL SOCIETY OF CHEMISTRY

PAPER

View Article Online
View Journal

Cite this: DOI: 10.1039/d5lf00353a

Unravelling chemical pathways of H_2 on Ga_2O_3 surfaces with spectro-electrochemistry

Krishna Teja Valeti, [a] Kazi Rifat Bin Rafiq, [ab] William A. Callahan, [c] Dino Klotz,[de] Andriy Zakutayev, [c] Ryan O'Hayre [a] and Anna F. Staerz *[a]

Received 10th November 2025,
Accepted 9th February 2026

DOI: 10.1039/d5lf00353a

rsc.li/RSCApplInter

This work highlights the capability of coupled spectroscopic and electrochemical techniques to probe dynamic surface processes under realistic operating conditions. By simultaneously employing *in situ* diffuse reflectance infrared Fourier transform spectroscopy (DRIFTS) and electrochemical impedance spectroscopy (EIS), we elucidate the mechanistic interaction between Ga_2O_3 and hydrogen under elevated temperatures in a low-oxygen environment. This novel spectro-electrochemical approach allows chemistry to be correlated with the surface charge density of Ga_2O_3. Our results reveal a concentration-dependent transition in reaction pathway. At low concentrations, hydrogen reacts with ambient oxygen to form surface hydroxyls. At intermediate concentrations, hydrogen interacts with surface adsorbed oxygen to generate hydroxyl groups along with reducing the surface. Finally, at high H_2 concentrations, hydrogen reduces both hydroxyls and surface oxygen, leading to a highly conductive grain surface. As a result, hydrides form on the reduced Ga_2O_3 surface. The gained insights are relevant for heterogeneous catalysis and gas sensing.

Introduction

Over the past two decades, catalyst characterization has transformed substantially, driven by the development of *in situ* and *operando* methodologies focused on identifying chemical species.[1] These techniques offer a major advantage over traditional *ex situ* or post-mortem analyses by enabling real-time observation of catalysts under working conditions.[2] Various spectroscopic methods, including infrared (IR), Raman, and X-ray photoelectron spectroscopy, have been used extensively used to study catalyst surface chemistry.[1,3] DRIFT spectroscopy has become a mainstay of *in situ* catalytic studies.[3] In DRIFT spectroscopy, using a complex mirror optics, a porous sample is irradiated with mid-IR light. The IR light that undergoes diffuse reflection is collected. The reflected light is focused to the detector. By comparing the reflected light intensity to that of the radiation source, absorption by the sample is identified. DRIFT spectroscopy is more suited for analysing surface chemical changes in operation conditions *versus* other IR methods, as it can be performed on opaque samples, it is highly surface-sensitive, and it requires no physical contact with the sample.[4,5]

During a reaction, the catalyst surface forms chemical bonds with reactants, facilitating the breaking of intramolecular bonds and the formation of new ones. It is widely understood that changes in the electron density of the catalyst surface can occur during operation. The importance of surface electronic structure was first identified in the 1960s by F. F. Wolkenstein, who examined the catalytic behaviour of semiconductor surfaces.[6] According to his theory, monitoring changes of the surface electron density during reactions should provide complementary information to studies focused on surface chemistry.[6] Building on our previous work on fuel cell materials, we have shown that impedance spectroscopy is ideally suited to gain information *in situ* about the electron density on the catalyst.[7] In impedance spectroscopy, a system in equilibrium is perturbed with an AC sinusoidal signal at different frequencies. From changes in the amplitude and phase shifts of the output signal, charge-transfer processes with varying time constants can be differentiated. The perturbation amplitude is selected so that the system remains in quasi-equilibrium, therefore, the measurement should not alter the catalytic behaviour.[8]

An example of an important problem in the field of surface science is the mechanism of the interaction between

[a] *Metallurgical and Materials Engineering, Colorado School of Mines, 1500 Illinois St, Golden, CO 80401, USA. E-mail: astaerz@mines.edu*
[b] *Mechanical Engineering, Colorado School of Mines, 1500 Illinois St, Golden, CO 80401, USA*
[c] *Materials Science Center, National Laboratory of the Rockies, Golden, Colorado 80401, USA*
[d] *WPI-International Institute for Carbon-Neutral Energy Research (I2CNER), Kyushu University, Japan*
[e] *Department of Materials Science and Engineering (DMSE), Massachusetts Institute of Technology (MIT), Cambridge, USA*

an oxide surface and gas molecule at operating conditions, for example interaction of Ga_2O_3 and hydrogen at elevated temperatures. The interaction, especially in a low oxygen background is relevant for both gas sensing and catalysis. Early work by Fleischer *et al.* found that porous Ga_2O_3 films could be used to reversibly detect high hydrogen concentrations in a nominally inert environment at high temperatures (~500 °C).[9,10] In catalysis, the formation and the reactivity of hydrogen adsorbed on Ga_2O_3 is important in the context of water–gas shift activity and its activity in methanol synthesis and methanol steam reforming.[9,11] While chemical species involved in catalysis have been extensively studied, the role of surface electron density in catalyst activity remains underexplored.[12]

Here we demonstrate the simultaneous measurement of diffuse reflectance Fourier transform infrared (DRIFT) and impedance spectroscopy and clarify the interaction of hydrogen with the Ga_2O_3 surface at elevated temperatures. Consistent with previous studies on Ga_2O_3, our DRIFT spectra show the formation of hydroxyl and hydride species, along with surface reduction. Using the novel set-up, we are able to advance the fundamental understanding of the reaction pathways. For the first time, we identified a switch in dominant reaction pathway with varying hydrogen concentration. At low concentrations, which had not yet been systematically examined in literature, we found that surface dipole formation is the prevailing mechanism. With increasing concentration, surface oxygen reacts with hydrogen to form hydroxyl groups. At high hydrogen concentrations, both the hydroxyl groups and surface oxygen react with hydrogen, likely leaving was water. This work serves as a proof of concept highlighting the usefulness of coupling DRIFT and impedance spectroscopy to study heterogeneous catalysts and gas sensor materials *in situ*.

Experimental methods

0.2 g of Ga_2O_3 powder (Sigma Aldrich 99% pure) was mixed with 130 μL of 1,2-propanediol to make a paste which was drop cast onto a commercially available alumina substrate (Newvision1981) with interdigitated gold electrodes (metal layer structure: Ti 0.1 μm/Cu 2 μm/Ni 1 μm/Au 1 μm respectively). The Au width is 180 μm and the gap is 220 μm. The layer was dried at 120 °C for 1 h and then heat treated at 500 °C. Scanning electron microscopy (SEM) was performed on the Ga_2O_3 layer using a FESEM JEOL 7000F with 20 kV acceleration voltage. X-ray diffractometry (XRD) was done using a Bruker Phaser XRD with a Cu Kα source.

For the *in situ* measurements, we used a custom measurement chamber machined out of aluminium equipped with a KBr window. The chamber is equipped with gold plated electrical probes and a Pt-resistive heater (Case Western). The exhaust oxygen concentration was measured using a Zirox SGM7 oxygen analyser. A current–voltage curve of the Ga_2O_3 layer at 500 °C in nominal nitrogen was measured using a Gamry 1000E potentiostat. The scan rate was 1 mV S^{-1}, and the measurement was conducted from 0 to +3 volts. The *in situ* impedance measurements were done under open circuit using a MFIA (Zurich Instruments) between 5 MHz to 50 mHz. The gaseous environment in the chamber was varied using a computer-controlled gas mixing system (five mass flow controllers SFC5500s, Sensirion). The total flow was maintained at 500 ml min^{-1} throughout the measurement. Hydrogen was dosed from a 1% H_2 tank balanced by nitrogen (General Air, 99.99%) and nitrogen (General Air, 99.99%) is used as the carrier gas. The complete *in situ* set-up is shown in Fig. 1a.

Measurement and data extraction

The concentration of hydrogen in the chamber was dosed in a stepwise manner from 0 to 10 000 ppm (1%). The concentration *versus* time profile is given in Fig. 1b. IR spectra and impedance were measured once the sensor had stabilized under each condition. The points at which the spectra were taken are shown by stars in Fig. 1b. Each IR spectrum was acquired by averaging 160 scans collected with a resolution of 4 cm^{-1}.

To evaluate the IR spectra, the relative absorbance was calculated. We reference the IR spectra taken during hydrogen exposure (purple stars in Fig. 1b) to the spectrum taken in the absence of hydrogen (green star). We selected this method as Olinger and Griffiths found that for DRIFTS measurements on absorbing samples, analysing the relative absorbance provides the best linear approximation of band intensity to adsorbate concentration, as shown in Fig. 2a.[13] Applying the method, absorbance bands that increase with hydrogen exposure are related to functional groups that have

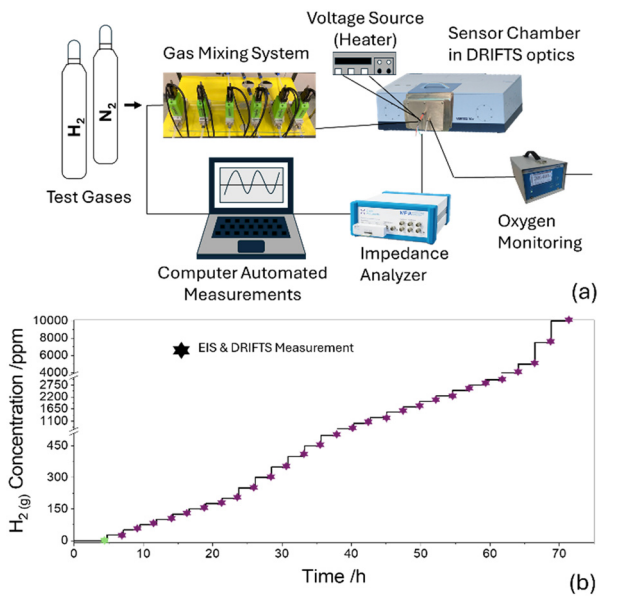

Fig. 1 (a) Schematic of the novel *in situ* spectro-electrochemical set-up. (b) Hydrogen concentration *versus* time profile used in this study. The IR and impedance spectra were measured at the points marked with a star.

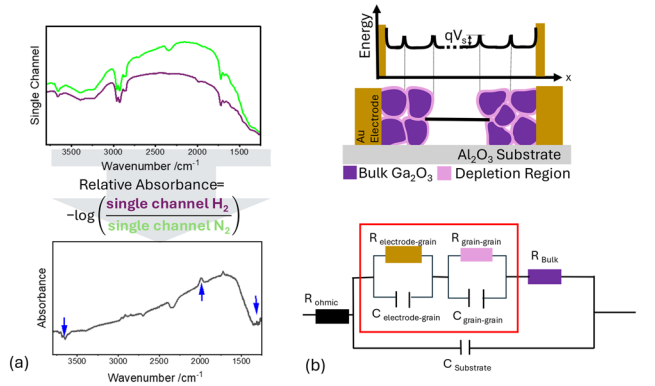

Fig. 2 (a) Schematic of the calculation used to calculate the relative absorbance spectra. (b) Schematic representation of the Ga_2O_3 depletion layer and the corresponding equivalent circuit.

formed because of the hydrogen exposure while absorbance bands that decrease with hydrogen exposure are either due to the removal or conversion of the associated surface species.

We use equivalent circuit modelling to extract meaningful information from the impedance spectra. A schematic of the physical system and the associated equivalent circuit model is shown in Fig. 2b. The Nyquist plots are given in the SI (S1–S3). Different processes contribute to the total impedance. Ga_2O_3 shows *n*-type semiconducting behaviour at elevated temperatures due to anion vacancies charge-compensated by electrons.[14] In the sensor field, highly porous *n*-type metal oxide-films operated in the presence of oxygen are thought to have a charge depletion region at grain surfaces as a result of oxygen chemisorption.[15] In the highly porous layers (not sintered) electrons must cross the potential barriers between adjacent grains to flow from one gold electrode to the other. In the equivalent circuit, these grain–grain barriers are modelled as capacitive elements in parallel with a resistor.

The Ga_2O_3 bulk is then modelled as the resistive element in series with the grain boundaries.[16–20] The electrode-grain contact depends on the work functions of both and is modelled as a capacitive element in parallel with a resistor. This component is in series with the bulk and grain–grain elements. In the depletion regime operation, the hundreds of grain–grain elements present in between the electrodes should dominate the total impedance and the contribution from electrode-grain contact should be negligible (Fig. 2b).[21–23]

The fits of the attained Nyquist plots using the equivalent circuit were done using *Z*-fit analysis (Z-view). The grain boundaries are modelled as a parallel resistor–capacitor circuit. The capacitance extracted for the surface reaction of the complete Ga_2O_3 layer using this equivalent circuit model from the *Z*-fit is found to vary with change in the resistance attributed to the grain–grain junction. This is in line with previous work in the sensor field.[20] The capacitance of the high frequency semicircle is in the picofarad range which has previously been attributed to the alumina substrate.[18–20]

Results

The porous Ga_2O_3 layer was characterized using SEM and XRD. The particles visible in SEM are <5 μm, see Fig. 3a. Assuming that this is the largest particle size, tens to hundreds of grain–grain junctions will be probed between the 250 μm interdigitated gold electrode gap. From the XRD pattern, as expected, the most stable β-Ga_2O_3 is the dominant phase in the sample.

To verify that the absorbance bands are not due to gaseous hydrogen or the interaction with other cell components, a reference IR spectrum in 10 000 ppm H_2 (reference state nominal nitrogen, ~90 ppm O_2 in the exhaust) was measured, see Fig. 4b. There are no significant increasing or decreasing bands visible in the IR spectra under these conditions.

In the measurement done at 500 °C, there are five discrete regions visible in the impedance results with increasing H_2 concentrations. These regions are also correlated with varying surface chemistry indicated in the DRIFT spectroscopy measurements. The relative absorbance IR spectra are shown in Fig. 5. For the impedance data, one parallel capacitance and resistance element was used that encompasses both the grain–grain and the electrode-grain contributions—corresponding to the red box shown in Fig. 2b. Under depletion region conditions, the grain–grain junctions will dominate the impedance. The grain–grain junction resistance (circles) and capacitance (triangles) extracted from the corresponding impedance data are shown in Fig. 6. In the

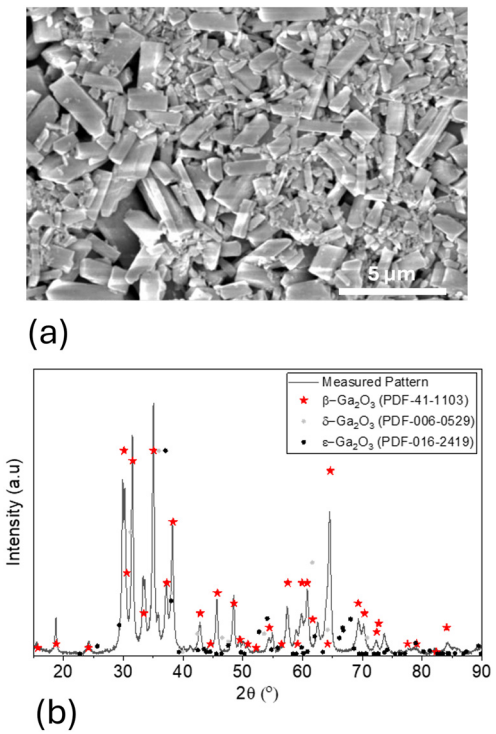

Fig. 3 (a) SEM image of the Ga_2O_3 sensitive layer surface is shown. (b) Pattern match analysis of β-Ga_2O_3.

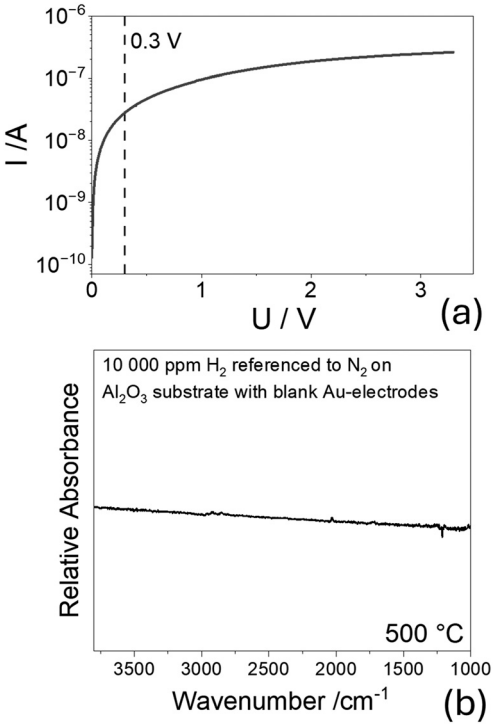

Fig. 4 (a) A current–potential curve was measured of the sensitive layer at 500 °C in nominal nitrogen. (b) A relative absorbance of the bare substrate with interdigitated Au-electrodes was calculated using the spectrum of the substrate at 500 °C in 1% H_2 referenced to that taken in the absence of hydrogen.

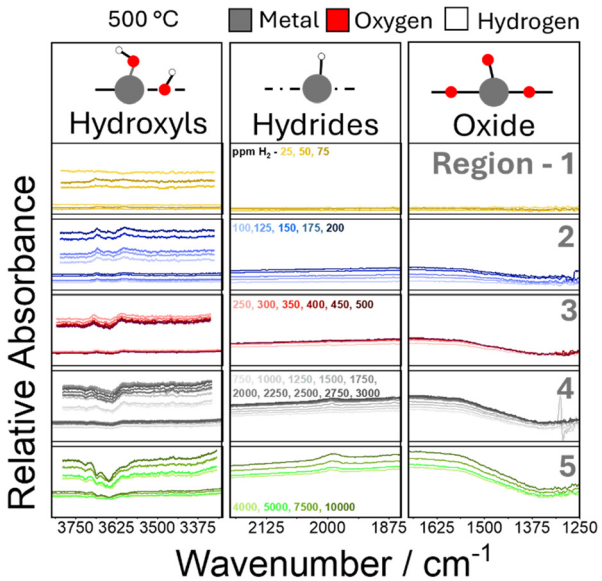

Fig. 5 DRIFT relative absorbance spectra overview of the Ga_2O_3 sample at 500 °C during exposure to different concentration of hydrogen in nominal nitrogen (~90 ppm O_2 measured in exhaust).

different regions, the increasing concentrations are indicated by increasing darkness of colour. The colours are matched between Fig. 5 and 6.

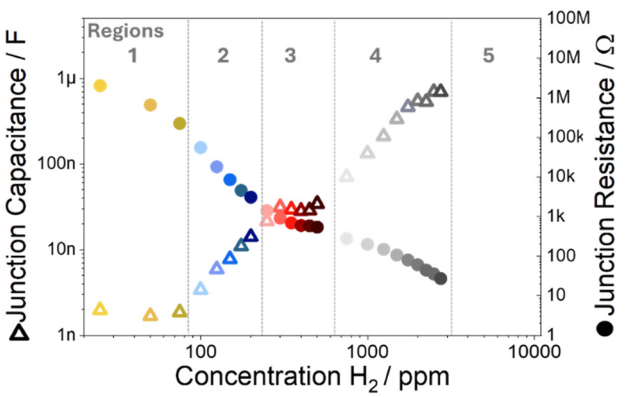

Fig. 6 Overview of junction resistance and capacitance extracted from the impedance measurements measured on the Ga_2O_3 sample at 500 °C simultaneously to the IR spectra.

1. Region one (<75 ppm hydrogen)

This region is in yellow in Fig. 5 and 6. In this concentration range there is a clear decrease in the resistance attributed to the grain–grain junctions, while the associated capacitance remains largely constant, Fig. 6. In the infrared spectra, only an increase in the bands attributed to surface hydroxyls are visible (between 3800 and 3350 cm^{-1}), Fig. 5.

2. Region two (100–200 ppm hydrogen)

This region is blue in Fig. 5 and 6. There is a clear decrease in the resistance attributed to the grain–grain junctions, and a concurrent increase in the associated capacitance. In the infrared spectra, with heightened hydrogen concentration, an increase in surface hydroxylation is accompanied by a broad decrease centred around ~1350 cm^{-1}. Although the assignment of bands in this region remains debated, this feature is commonly attributed to surface metal–oxygen vibrations.[24,25]

3. Region three (250–500 ppm hydrogen)

This region is marked in red in Fig. 5 and 6. In this region there appears to be saturation of the initial reactive sites on the Ga_2O_3 surface. There is no significant change in the resistance or the capacitance attributed to the grain–grain junction with increasing hydrogen concentration. This is mirrored by the IR spectra. There is no significant increase in the bands associated with hydroxyls and no further decrease in the broad band centred around 1350 cm^{-1} with increasing hydrogen.

4. Region four (750–3000 ppm hydrogen)

This region is marked in grey in Fig. 5. A steeper decrease in the grain–grain junction resistance and concurrent increase in the grain–grain junction capacitance is observed. This is attributed to the reduction of surface hydroxyl groups and further reduction of the metal–oxide surface observed in IR.

5. Region five (4000–10 000 ppm hydrogen)

This region is marked in green in Fig. 5. The resistance and capacitance associated with the grain–grain junction is no longer visible in the impedance measurements, therefore there are no symbols visible in Fig. 3b. In the IR there is a stronger decrease visible in both the metal–oxygen and hydroxyl region. Additionally, there is a clear and continuous increase in a broad band attributed to surface hydrides.

The results of the measurement done at 500 °C are summarized in Table 1.

The sample was let to recover in nitrogen (~90 ppm residual O_2). The total impedance recovered to the same level observed during the initial measurement in nitrogen before hydrogen testing. The initial and final impedance at 500 °C are summarised in Fig. S8. This reversible recovery confirms the physical stability of the sample under the test conditions. The measurement was repeated at 475 °C and at 450 °C. An overview of the DRIFT spectra and the corresponding resistance and capacitance behaviour is given in the SI S4 and S5. The change in intensity of the band attributed to the reduction and of that attributed to hydride formation were extracted from the single channel for each hydrogen concentration. The change in band intensity *versus* the change of the inter-junction resistance for all three temperatures is summarized in Fig. 7a and b. The hydroxyl region was not included as there is a significant overlap between bands which at times are both increasing and decreasing.

In Fig. 7a, there is a clear correlation between the decrease in junction resistance and the decreasing band associated with surface reduction. The result is very similar for all three temperatures. In Fig. 7b, there is a clear difference between the different temperatures. From the enlarged inset, it is clear that the relation between the IR band intensity and the resistance is not monotonous.

We extracted the resistance values at three different concentrations representative of the regions that show different dominant catalytic behaviour in all three temperatures. For region one (yellow in Fig. 5), we selected 50 ppm; for region two (blue in Fig. 5) 150 ppm; for region four (grey in Fig. 5) 2000 ppm. We then used these values to determine the activation energy of the different processes using the following relation:

$$\ln R = \ln R_0 + \frac{E_A}{k_B} \times \frac{1}{T} \quad (1)$$

An Arrhenius behaviour of the resistance was assumed, and the plots are shown in Fig. 7c.[26]

The geometric capacitance contributed by the substrate remained largely unchanged throughout the hydrogen concentrations, given in S6. The overview of the bulk and contact resistances at different temperatures is given in S7.

Discussion

By measuring DRIFT and impedance spectroscopy simultaneously we identify four different dominant reaction pathways depending on the hydrogen concentration. For the three regions in which we could extract an inter-junction resistance, activation energies were determined. Generally, resistance is defined as:

$$R = \frac{L}{nq\mu A} \quad (2)$$

with L (length), (n) carrier concentration, (q) elementary charge, and (μ) is the mobility. Mobility is expected to have a temperature dependence. The information related to the reaction pathways is contained in both the surface carrier concentration and the geometry (length and area) of the depletion region. The surface potential is known to influence the surface carrier concentration. Surface potential in turn is influenced by electron affinity (surface dipoles) and changes in the work function. Since the surface chemistry can influence both the electron affinity and the work function, changes in grain–grain resistance should be intimately related to these processes.[15,21] Nonetheless, although changes in the grain–grain equilibrium resistance under hydrogen exposure at different temperatures should reflect changes in surface chemistry, it will also be influenced by variations in carrier mobility (temperature and defect concentration dependent). As a result, although the difference in activation energies clearly indicates a change in dominant pathways, the absolute values of the activation energies should be viewed as approximations.

The results indicate that in region one (low hydrogen concentrations) dipole formation in the form of hydroxyls is dominant. As no reduction is visible in the IR and no significant capacitance change was seen, this dipole

Table 1 Summary of chemical pathways

Chemical Pathways at 500 °C							
		Inter-grain junction		DRIFT rel. absorbance bands			
Region	H_2/ppm	Capacitance	Resistance	Hydroxyl	Hydride	M–O	Chemical pathway
1	<75	—	↓	↑	—	—	Dipole formation
2	100–200	↑	↓	↑	—	↓	Reduction through hydroxylation
3	250–500	—	—	—	—	—	Saturation
4	750–3000	↑	↓	↓	↑	↓	Reduction
5	4000–10 000	NA	NA	↓	↑	↓	Total reduction

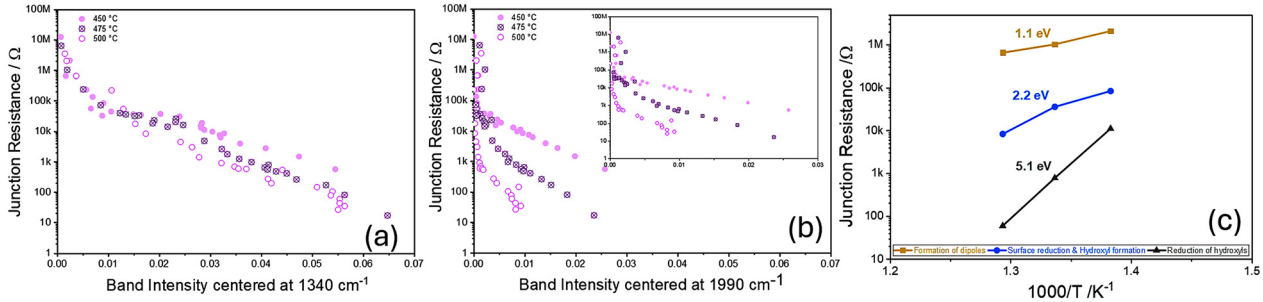

Fig. 7 (a) IR band intensity centred at 1340 cm^{-1} (associated with surface reduction) is plotted against the inter-junction resistance. (b) IR band intensity centred at 1990 cm^{-1} (associated with surface hydrides) is plotted against the inter-junction resistance. (Inset) Enlarged view of band intensity at 1990 cm^{-1} *vs.* inter-junction resistance. (c) Arrhenius plots of the inter-junction resistance in three different concentration regions.

formation is likely due to the combined interaction and adsorption of hydrogen and the residual oxygen (~90 ppm O_2). The activation energy of ~1 eV calculated from the Arrhenius plot for this process is in line with those reported in literature for the catalytic dissociation of water on metal oxide surfaces.[27]

The processes found to dominate at higher hydrogen concentrations were associated with higher activation energies determined from the Arrhenius plots. While hydroxyl formation is still visible in the second region, it is now accompanied by a decrease in the IR region associated with gallium oxygen bonds. In line with a surface reduction, the decrease of resistance is accompanied by an increase in capacitance. This behaviour aligns with the relationship derived by Kappler for capacitance and resistance of grain–grain junctions. Based on his modelling, in *n*-type semiconductors assuming a surface depletion mechanism, the resistance is exponentially proportional to band bending while the capacitance is inversely dependent on the square root. The extrapolated activation energy of 2.2 eV is within the reported range associated with hydroxylation of surface oxygens on oxides.[28]

At 500 °C, between 250 and 500 ppm H_2, there is no substantial change in resistance or capacitance. In the IR both the reduction and the hydroxyl group formation have saturated, *i.e.* no change with increasing hydrogen concentration. Above 750 ppm (at 500 °C), the process with the highest activation energy dominates. A clear decrease in the IR region associated with gallium oxygen bonds is now accompanied by a decrease in surface hydroxyls. In this region the resistance is decreasing, and the capacitance is increasing. The dependence of resistance and capacitance on the concentration is weaker (less steep slope in Fig. 6) than for lower H_2 concentrations.

In this region, the formation of hydrides is visible in the IR. The formation of gallium hydrides, which are $-H^-$ species, indicates that the grain surface is strongly reduced and becomes electron rich. This enables transfer of electrons to hydrogen to form hydrides. As a result, the grain–grain junctions no longer exhibit an intergranular potential barrier but instead offer a high conductivity pathway. We believe that in this accumulation regime the electrode-grain contact is responsible for the low frequency process. This is supported by the varying, concentration-dependent slope of both the capacitance and the resistance. The corresponding equivalent circuit for this regime is shown in Fig. 8.[29] Upon further increasing the hydrogen concentration, the electrode-grain contact appears to become ohmic. The overall resistance of the sample is now very low (<100 Ω), and equivalent circuit fits are no longer possible.

We believe that the influence of the strong surface reduction masks the electronic effect of the hydrides. The dominant influence of surface reduction on the resistance change is supported by the relations shown in Fig. 7a and b. Our results also indicate that hydrides cannot be used as a proxy for the level of surface reduction. The band intensity associated with hydrides (related to concentration) is highest at 450 °C. Our results indicate however that the surface is more heavily reduced in high hydrogen concentrations at 500 °C, indicated by low junction resistance and higher intensity of the band associated with reduction. This is likely due to a decrease in the stability of surface hydrides at higher temperatures. The high activation energy, ~5 eV is within the range predicted for surface oxygen vacancy formation, which is necessary for hydride formation.[30]

The transition points between the different regions shift to higher concentrations at lower temperatures. The grain-electrode contact is visible within the entire hydrogen concentration range at temperatures below 500 °C. This behaviour is expected as chemical activity is inherently linked to temperature; accordingly, a higher level of hydrogen should be required to reduce beyond the surface at 450 °C and 475 °C than at 500 °C.

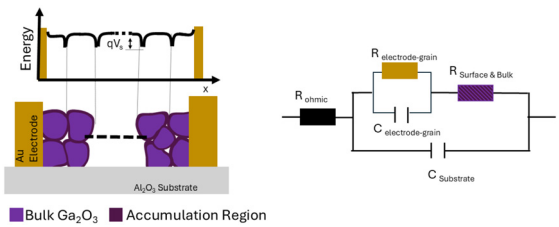

Fig. 8 Schematic representation of the Ga_2O_3 accumulation layer and the corresponding equivalent circuit.

Conclusions

This work demonstrates the effectiveness and versatility of combining impedance with DRIFT spectroscopy to study the complex interactions that occur at metal oxide – gas interfaces. By simultaneously monitoring both charge transfer dynamics and surface chemical processes, we successfully elucidate how hydrogen interacts with the Ga_2O_3 surface. Our results reveal that these interactions are strongly dependent on hydrogen concentrations. There are varying dominant mechanisms at different exposure levels.

Specifically, the study provides conclusive evidence that surface reduction processes drive the pronounced changes in electrical conductivity observed in polycrystalline Ga_2O_3 films at elevated temperatures (around 500 °C) when exposed to hydrogen in otherwise inert atmospheres. Our results also indicate that the presence of low levels of residual oxygen is responsible for the reversibility of this change in resistance.

This work validates the performance and versatility of the custom-designed *in situ* pectro-electrochemical system. The results also clearly demonstrate that the electron theory of catalysis is not in conflict with mechanistic studies that focus on the evolution of chemical species. Instead, the approaches deal with different aspects of catalysis. As surface chemistry and electronic behaviour is intimately linked, their simultaneous study offers complementary insights into the same catalytic processes. In the future, the presented methodology can be extended to investigate a wide variety of materials, at elevated temperatures (<500 °C) and environments, conditions relevant for work in heterogeneous catalysis, sensing, and energy conversion applications.

Author contributions

Krishna Teja Valeti: conceptualization, validation, formal analysis, data curation, visualization, writing – original draft, Kazi Rifat Bin Rafiq: investigation, William A. Callahan: writing – review & editing, Dino Klotz: methodology and formal analysis, Andriy Zakutayev: funding acquisition, project administration, Ryan O'Hayre: funding acquisition, writing – review & editing, Anna Staerz: funding acquisition, resources, conceptualization, supervision, writing – review & editing.

Conflicts of interest

There are no conflicts to declare.

Data availability

All raw data supporting the findings of this study are provided in the accompanying folder. The folder includes the Z-view readable impedance data for all measurements, simultaneously measured single channel DRIFTS data and the XRD data. The data are organized in easily readable Excel and text file formats to facilitate transparency and reproducibility.

Supplementary information (SI) is available. See DOI: https://doi.org/10.1039/d5lf00353a.

Acknowledgements

This work was authored in part by the National Laboratory of the Rockies (NLR) for the U.S. Department of Energy (DOE) under Contract No. DE-AC36-08GO28308. Funding is provided by the Office of Critical Minerals and Energy Innovation (CMEI), Advanced Materials & Manufacturing Technologies Program (AMMTO). Some of the work was performed in following core facility, which is a part of Colorado School of Mines' Shared Instrumentation Facility Electron Microscopy: RRID:SCR_022048. The views expressed in the article do not necessarily represent the views of the DOE or the U.S. Government.

References

1 F. Zaera, In-situ and operando spectroscopies for the characterization of catalysts and of mechanisms of catalytic reactions, *J. Catal.*, 2021, **404**, 900–910, DOI: 10.1016/j.jcat.2021.08.013.

2 S. Sharma, F. Maurer, P. Lott and T. L. Sheppard, Unlocking the Mysteries of Technical Catalyst Deactivation: A View from Space, *ChemCatChem*, 2024, **16**(14), DOI: 10.1002/cctc.202301655.

3 H. Hoser, A. Innocenti, A. Riva and F. Trifiró, Catalytic activity of HZSM-5 zeolite in 1-butene conversion. Diffusive reflectance-IR spectroscopic study in a flow system, *Appl. Catal.*, 1987, **30**(1), 11–20, DOI: 10.1016/S0166-9834(00)81007-6.

4 A. Urakawa, T. Bürgi and A. Baiker, Sensitivity enhancement and dynamic behavior analysis by modulation excitation spectroscopy: Principle and application in heterogeneous catalysis, *Chem. Eng. Sci.*, 2008, **63**(20), 4902–4909, DOI: 10.1016/j.ces.2007.06.009.

5 S. Harbeck, A. Szatvanyi, N. Barsan, U. Weimar and V. Hoffmann, DRIFT studies of thick film un-doped and Pd-doped SnO2 sensors: temperature changes effect and CO detection mechanism in the presence of water vapour, *Thin Solid Films*, 2003, **436**(1), 76–83, DOI: 10.1016/S0040-6090(03)00512-1.

6 T. Wolkenstein, The Electron Theory of Catalysis on Semiconductors, *Adv. Catal.*, 1960, 189–264, DOI: 10.1016/S0360-0564(08)60603-3.

7 A. Staerz, H. G. Seo, D. Klotz, D. S. Kim, J. M. LeBeau and H. L. Tuller, The Influence of Cr-Additives on the Polarization Resistance of Praseodymium-Doped Ceria Cathodes for Solid Oxide Fuel Cells, *J. Electrochem. Soc.*, 2022, **169**(4), 044530, DOI: 10.1149/1945-7111/ac67b2.

8 F. Schipani, D. R. Miller, M. A. Ponce, C. M. Aldao, S. A. Akbar and P. A. Morris, Electrical Characterization of Semiconductor Oxide-Based Gas Sensors Using Impedance Spectroscopy: A Review, *Rev. Adv. Sci. Eng.*, 2016, **5**(1), 86–105, DOI: 10.1166/rase.2016.1109.

9 R. Pohle, M. Fleischer and H. Meixner, In situ infrared emission spectroscopic study of the adsorption of H2O and hydrogen-containing gases on Ga2O3 gas sensors,

Sens. Actuators, B, 2000, **68**(1–3), 151–156, DOI: 10.1016/S0925-4005(00)00476-7.

10 M. Fleischer and H. Meixner, Sensing reducing gases at high temperatures using long-term stable Ga2O3 thin films, *Sens. Actuators, B*, 1992, **6**(1–3), 257–261, DOI: 10.1016/0925-4005(92)80065-6.

11 W. Jochum, S. Penner, K. Fottinger, R. Kramer, G. Rupprechter and B. Klotzer, Hydrogen on polycrystalline β-Ga2O3: Surface chemisorption, defect formation, and reactivity, *J. Catal.*, 2008, **256**(2), 268–277, DOI: 10.1016/j.jcat.2008.03.019.

12 M. Argyle and C. Bartholomew, Heterogeneous Catalyst Deactivation and Regeneration: A Review, *Catalysts*, 2015, **5**(1), 145–269, DOI: 10.3390/catal5010145.

13 J. M. Olinger and P. R. Griffiths, Quantitative effects of an absorbing matrix on near-infrared diffuse reflectance spectra, *Anal. Chem.*, 1988, **60**(21), 2427–2435, DOI: 10.1021/ac00172a022.

14 K. Yamaguchi, First principles study on electronic structure of β-Ga2O3, *Solid State Commun.*, 2004, **131**(12), 739–744, DOI: 10.1016/j.ssc.2004.07.030.

15 N. Barsan, D. Koziej and U. Weimar, Metal oxide-based gas sensor research: How to?, *Sens. Actuators, B*, 2007, **121**(1), 18–35, DOI: 10.1016/j.snb.2006.09.047.

16 N. Barsan and U. Weimar, Conduction Model of Metal Oxide Gas Sensors, *J. Electroceram.*, 2001, **7**(3), 143–167, DOI: 10.1023/A:1014405811371.

17 G. Heiland, Homogeneous semiconducting gas sensors, *Sens. Actuators*, 1981, **2**, 343–361, DOI: 10.1016/0250-6874(81)80055-8.

18 C. E. Simion, F. Schipani and A. Papadogianni, *et al.*, Conductance Model for Single-Crystalline/Compact Metal Oxide Gas-Sensing Layers in the Nondegenerate Limit: Example of Epitaxial SnO_2 (101), *ACS Sens.*, 2019, **4**(9), 2420–2428, DOI: 10.1021/acssensors.9b01018.

19 F. Schipani, M. A. Ponce, E. Joanni, F. J. Williams and C. M. Aldao, Study of the oxygen vacancies changes in SnO2 polycrystalline thick films using impedance and photoemission spectroscopies, *J. Appl. Phys.*, 2014, **116**(19), DOI: 10.1063/1.4902150.

20 J. Kappler, *Characterisation of high-performance SnO_2 gas sensors for CO detection by in situ techniques*, 2001.

21 C. Malagù, V. Guidi, M. Stefancich, M. C. Carotta and G. Martinelli, Model for Schottky barrier and surface states in nanostructured n-type semiconductors, *J. Appl. Phys.*, 2002, **91**(2), 808–814, DOI: 10.1063/1.1425434.

22 L. A. M. Lyle, Critical review of Ohmic and Schottky contacts to β-Ga2O3, *J. Vac. Sci. Technol., A*, 2022, **40**(6), DOI: 10.1116/6.0002144.

23 W. A. Callahan, E. Supple and D. Ginley, *et al.*, Ultrathin stable Ohmic contacts for high-temperature operation of β - Ga2O3 devices, *J. Vac. Sci. Technol., A*, 2023, **41**(4), DOI: 10.1116/6.0002645.

24 A. Davydov, *Molecular Spectroscopy of Oxide Catalyst Surfaces*, Wiley, 2003, DOI: 10.1002/0470867981.

25 A. Davydov, K. T. Chuang and A. R. Sanger, Mechanism of H_2S Oxidation by Ferric Oxide and Hydroxide Surfaces, *J. Phys. Chem. B*, 1998, **102**(24), 4745–4752, DOI: 10.1021/jp980361p.

26 K. Charles, *Introduction to solid state physics*, Wiley, 2005.

27 H.-Y. Su, K. Sun and X.-K. Gu, *et al.*, Finding Key Factors for Efficient Water and Methanol Activation at Metals, Oxides, MXenes, and Metal/Oxide Interfaces, *ACS Catal.*, 2022, **12**(2), 1237–1246, DOI: 10.1021/acscatal.1c03405.

28 A. Ruiz Puigdollers, F. Illas and G. Pacchioni, Reduction of Hydrogenated ZrO_2 Nanoparticles by Water Desorption, *ACS Omega*, 2017, **2**(7), 3878–3885, DOI: 10.1021/acsomega.7b00799.

29 N. Barsan, J. Rebholz and U. Weimar, Conduction mechanism switch for SnO2 based sensors during operation in application relevant conditions; implications for modeling of sensing, *Sens. Actuators, B*, 2015, **207**, 455–459, DOI: 10.1016/j.snb.2014.10.016.

30 L. Qin, Z. Cheng, M. Guo, J. A. Fan and L.-S. Fan, Morphology evolution and nanostructure of chemical looping transition metal oxide materials upon redox processes, *Acta Mater.*, 2017, **124**, 568–578, DOI: 10.1016/j.actamat.2016.11.025.